CRYSTALLOGRAPHIC STUDY OF SOLVATES AND SOLVATE HYDRATES OF AN ANTIBACTERIAL FURAZIDIN

Liāna Orola[1], Anatoly Mishnev[2], Dmitrijs Stepanovs[2], and Agris Bērziņš[1*]

[1]*Faculty of Chemistry, University of Latvia, Jelgavas iela 1, LV-1004, Riga, Latvia.*

[2]*Latvian Institute of Organic Synthesis, Aizkraukles iela 21, LV-1006 Riga, Latvia.*

* *agris.berzins@lu.lv*

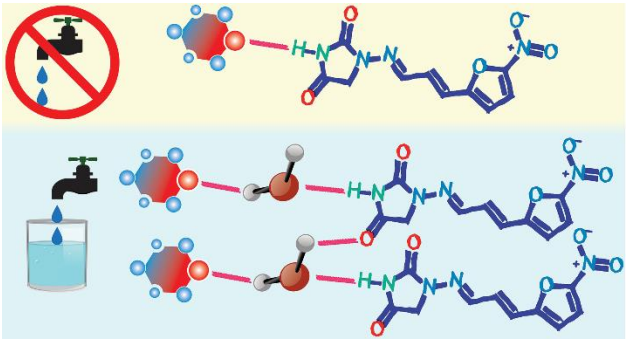

ABSTRACT

In this study we present a detailed crystallographic analysis of multiple solvates of an antibacterial furazidin. Solvate formation of furazidin was investigated by crystallizing it from pure solvents and solvent-water mixtures. Crystal structure analysis of the obtained solvates and computational calculations were used to identify the main factors leading to the intermolecular interactions present in the solvate crystal structures and resulting in formation of the observed solvates and solvate hydrates. Furazidin forms pure solvates and solvate hydrates with solvents having large hydrogen bond acceptor propensity and with a hydrogen bond donor and acceptor formic acid. In solvate hydrates the incorporation of water allows formation of additional hydrogen bonds and results in more efficient hydrogen bond network in which water is "hooking" the organic solvent molecule, and this slightly reduces the cut-off of solvent hydrogen bond acceptor propensity required for obtaining a solvate. The crystal structures of all pure solvates are formed from molecule layers and in almost all structures solvent is hydrogen bonded to the furazidin, but the packing in each solvate is unique. In contrast, the hydrogen bonding and packing in most solvate hydrates are nearly identical.

INTRODUCTION

It is well known that roughly 40-70% of small organic molecules can form different solid phases[1-2], including single component phases (polymorphs) and multiple component phases such as hydrates and solvates, co-crystals, solid solutions etc. Because of a considerable practical interest by the pharmaceutical industry formation and characterization of such phases is perhaps the best explored for pharmaceutical compounds[3]. A recent survey of Cambridge Structural Database[4] found than among thousands of different crystal structures formed by drug compounds 19.9% are hydrates, 8.6% single-solvent solvates and 1.5% heterosolvates (phases that include two or even more[5-8] different solvent molecules) containing water. Statistical analysis of crystal structures of various solvates and hydrates have revealed that the most important factors driving the hydrate and solvate formation are the size and branching of the molecules, followed by the hydrogen bonding ability[9]. This agrees with more general observations that solvate formation in most cases occur because of the ability of solvent to compensate unsatisfied potential intermolecular interactions between the host molecules and the ability to decrease the void space and/or lead to more efficient packing[10-12]. The most solvates include contributions from both of these driving forces[10].

Most of the heterosolvates are stoichiometric solvate hydrates, i.e. contain organic solvent and water, and both solvent molecules have a significant role in the formation of the hydrogen bonding network. Examples for compounds forming such solvates are olanzapine[13], bosutinib[14], stanozolol[15], 3,5-dihydroxybenzoic acid[16-17], cholic acid[18-19], deoxycholic acid[20-21] etc. There are also many heterosolvates containing two different organic solvents in well-defined crystal structure sites[22-25]. Additionally, in part of the heterosolvates solvent molecules are located in channels or other large cavities without specific requirements for solvate shape and size or even interactions[26-27].

In general, the reason for facile inclusion of water in the crystal structures is well known and is the small size, orientational freedom and versatile hydrogen bonding capabilities of water molecules[28], as water can act as a hydrogen bond acceptor and donor. The latter ability explains its incorporation in the solvate hydrates, as most organic solvates only have a hydrogen bond acceptor functionality. For example, for 3,5-dihydroxybenzoic acid solvate hydrates it is concluded that incorporation of water in hydrogen bonding network provides binding sites for other solvent molecules, as solvent molecules hydrogen bond to the water[16-17].

In this study we explored the solvate formation of furazidin (FUR, 1-[(E)-[(E)-3-(5-nitrofuran-2-yl)prop-2-enylidene]amino]imidazolidine-2,4-dione, molecular structure given in Figure 1), also know under the name of furagin. FUR is a nitrofurantoin analogue with an antibacterial activity[29] frequently used in the treatment of urinary tract infections mainly in eastern European countries.[30]

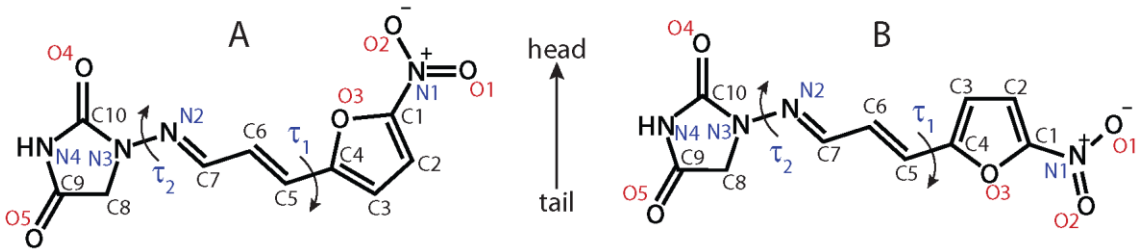

Figure 1. Molecular structure of FUR conformers A and B with numbering of non-hydrogen atoms, labelling of flexible torsion angles and head and tail designation as used in this study.

Furazidin is known to exist in two polymorphs I and II[31-32] as well as two solvate hydrates: THF solvate hydrate (CSD refcode ASATIZ) and DMF solvate hydrate (ASATOF)[33]. In our performed crystallization experiments of FUR formation of several pure solvates and additional solvate hydrates was observed. The aim of this study was therefore to use the crystal structure analysis and computational calculations to investigate the factors resulting in formation of FUR solvates and solvate hydrates and identify the differences in structures formed by different solvents.

2. Experimental

Crystallization

Furazidin was donated by JSC Olainfarm (Olaine, Latvia). Other reagents were purchased from commercial sources and used as received. FUR was crystallized from several solvents providing acceptable solubility for crystallization. These were aprotic polar solvents (DMF, DMA, DMSO, acetone, acetonitrile, nitromethane, ethyl acetate), electron pair donor solvents (THF, 1,4-dioxane, methyl tert-butyl ether), formic acid, acetic acid, their mixtures and their mixtures with water. Solvate formation was observed from DMF, DMA, DMSO, 1,4-dioxane, THF and formic acid. Crystallization from these solvents and their mixtures with water was investigated more extensively, by performing multiple crystallizations in different conditions (cooling crystallization, evaporation crystallization) and using different solvent ratios for solvent-water mixtures.

Solvates of dimethylformamide (FUR·DMF) and dimethylacetamide (FUR·DMA) were obtained by crystallizing 50 mg of FUR from the respective solvent (5 mL) at a room temperature. To obtain a DMF solvate hydrate (FUR·DMF·H_2O) 50 mg FUR was dissolved in a hot 4:1 mixture (5 mL) of DMF and water and allowed to crystallize at a room temperature. FUR solvate of 1,4-dioxane (FUR·DIOX) was acquired by dissolving 50 mg of FUR in a hot 1,4-dioxane (18 mL) and crystallizing at a room temperature. A 1,4-dioxane solvate hydrate (FUR·DIOX·H_2O) was prepared by dissolving 50 mg of FUR in a hot 9:1 mixture (10 mL) of 1,4-dioxane and water and crystallizing at a room temperature. A formic acid solvate (FUR·FA) was prepared by dissolving 70 mg FUR in a hot formic acid (2 mL) followed by slow evaporation at 5 ºC temperature. To obtain a formic acid solvate hydrate

(FUR·FA·H_2O) 50 mg FUR was dissolved in a hot 1:1 mixture (10 mL) of formic acid and water and allowed to crystallize at a room temperature. A tetrahydrofuran solvate hydrate (FUR·THF·H_2O) was obtained by dissolving 50 mg FUR in a hot 9:1 mixture (16 mL) of THF and water followed by slow evaporation at a room temperature. Dimethyl sulfoxide solvate polymorph I (FUR·DMSO I) was prepared by crystallizing 50 mg of FUR from DMSO (5 mL) at a room temperature. A crystallization of 200 mg of FUR from DMSO (10 mL) produced crystals of DMSO solvate polymorph II (FUR·DMSO II) at a room temperature. DMSO solvate polymorph III (FUR·DMSO III) was obtained by crystallizing 100 mg of FUR from DMSO (5 mL) at a room temperature.

Solvate characterization

X-ray powder diffraction (XRPD) patterns were measured at ambient temperature on a D8 Advance (Bruker) diffractometer using copper radiation (CuK_α) at the wavelength of 1.54180 Å, equipped with a LynxEye position sensitive detector. The tube voltage and current were set to 40 kV and 40 mA. The divergence slit was set at 0.6 mm and the antiscatter slit was set at 8.0 mm. The diffraction patterns were recorded using a 0.2s/0.02° scanning speed from 3° to 35° on 2θ scale.

The differential scanning calorimetry/thermogravimetry (DSC/TG) analysis was performed with TGA/DSC2 (Mettler Toledo). Open 100 µL aluminum pans were used. Heating of the samples from 25 to 300°C was performed at a 10°C·min^{-1} heating rate. Samples of 5–10 mg mass were used, and the nitrogen flow rate was 100±10 mL·min^{-1}.

Single Crystal X-ray Diffraction (SCXRD)

SCXRD data of all solvates except for FUR·DMSO III, FUR·DMF and FUR·DMA were measured with a Nonius Kappa CCD diffractometer (Bruker AXS GmbH, Germany) with MoKα radiation (0.71073 Å). Data were collected at 190 K (173 for FUR·DIOX) maintained using the Oxford Cryosystems Cryostream Plus equipment. Data reduction was performed with the DENZO/SCALEPACK. Crystal structures were solved by direct methods with SHELXS-97, refinement was performed by SHELXL-97[34].

SCXRD data of FUR·DMSO III, FUR·DMF and FUR·DMA were measured on a XtaLAB Synergy-S Dualflex diffractometer (RIGAKU Oxford Diffraction) equipped with a HyPix6000 detector and a microfocus sealed X-ray tube with Mo Kα radiation (λ = 0.7107 Å). A single crystal with dimensions of <0.1 × <0.1 × <0.1 mm^3 was fixed with oil in a nylon loop of a magnetic CryoCap and set on a goniometer head. Samples were measured at 293 K (170 K for FUR·DMF). Data collection and reduction were performed with the CrysAlisPro 1.171.40.35a software. Structure solution and refinement were performed with AutoChem3.0 and SHELXL[34] software that are parts of the CrysAlisPro suite. Further details are provided in Table 1 and Table S1, Supporting Information.

Table 1. Crystallographic data of FUR solvates and solvate hydrates

Phase	FUR·DMSO I	FUR·DMSO II	FUR·DMSO III	FUR·DMF	FUR·DMF·H_2O
Reference	CCDC 2222724	CCDC 2222725	CCDC 2121374	CCDC 2121392	ASATOF
Chemical formula	$C_{10}H_8N_4O_5 \cdot C_2H_6OS$	$C_{10}H_8N_4O_5 \cdot C_2H_6OS$	$C_{10}H_8N_4O_5 \cdot C_2H_6OS$	$C_{10}H_8N_4O_5 \cdot C_3H_7NO$	$C_{10}H_8N_4O_5 \cdot C_3H_7NO \cdot H_2O$
M_r (g mol^{-1})	342.33	342.33	342.33	337.30	355.32
Crystal system,	Monoclinic	Orthorhombic	Monoclinic	Orthorhombic	Monoclinic
Space group	$P2_1/c$	$Pc2_1n$	$P2_1/c$	$Pna2_1$	$P2_1/m$
Temperature (K)	190	190	293	170	190
a (Å)	19.8657(15)	6.77930(10)	15.7279(2)	21.7209(4)	6.3942(3)
b (Å)	6.1143(4)	18.0943(3)	10.8768(2)	6.9307(2)	6.3182(3)
c (Å)	12.9970(7)	37.2406(7)	8.92710(10)	41.2473(7)	20.3275(14)
α (º)	90	90	90	90	90
β (º)	103.489(2)	90	92.5670(10)	90	90.827(2)
γ (º)	90	90	90	90	90
V (Å^3)	1535.13(17)	4568.18(13)	1525.62(4)	6209.4(2)	821.14(8)
Z, Z'	4, 1	12, 3	4, 1	16, 4	2, 0.5
Calculated density (g cm^{-3})	1.481	1.493	1.490	1.443	1.437
Final R_1 ($F^2>2\sigma F^2$)	0.074	0.075	0.043	0.0651	0.068

Table 1. *Continued.*

Phase	FUR·DIOX	FUR·DIOX·H_2O	FUR·DMA	FUR·FA	FUR·FA·H_2O	FUR·THF·H_2O
CCDC number	CCDC 2122176	CCDC 2122145	CCDC 2122147	CCDC 2222740	CCDC 2122135	ASATIZ
Chemical formula	$C_{10}H_8N_4O_5 \cdot 0.5(C_4H_8O_2)$	$C_{10}H_8N_4O_5 \cdot 0.5(C_4H_8O_2) \cdot H_2O$	$C_{10}H_8N_4O_5 \cdot C_4H_9NO$	$C_{10}H_8N_4O_5 \cdot CH_2O_2$	$C_{10}H_8N_4O_5 \cdot CH_2O_2 \cdot H_2O$	$C_{10}H_8N_4O_5 \cdot C_4H_8O \cdot H_2O$
M_r (g mol^{-1})	308.26	326.27	351.32	310.23	328.25	354.32
Crystal system,	Monoclinic	Triclinic	Orthorhombic	Orthorhombic	Triclinic	Triclinic
Space group	$P2_1/c$	$P\bar{1}$	$Pca2_1$	$Pnma$	$P\bar{1}$	$P\bar{1}$
Temperature (K)	173	190	293	190	190	190
a (Å)	7.3597(2)	6.3974(2)	11.5290(4)	6.4668(3)	5.9110(2)	6.4307(3)
b (Å)	17.3004(4)	7.5217(3)	16.6013(7)	6.0446(3)	10.4468(3)	10.1436(4)
c (Å)	10.6798(3)	15.7099(8)	8.7057(2)	33.1560(15)	12.7190(6)	13.9982(7)
α (º)	90	102.824(2)	90	90	68.1670(10)	107.295(2)
β (º)	92.4540(10)	96.754(2)	90	90	78.7620(10)	96.530(2)
γ (º)	90	97.839(3)	90	90	83.954(2)	103.518(1)
V (Å^3)	1358.57(6)	721.60(5)	1666.24(10)	1296.04(11)	714.63(5)	831.00(7)
Z, Z'	4, 1	2, 1	4, 1	4, 0.5	2, 1	2, 1
Calculated density (g cm^{-3})	1.507	1.502	1.400	1.590	1.525	1.416
Final R_1 ($F^2>2\sigma F^2$)	0.083	0.051	0.045	0.053	0.047	0.048

Structure analysis

Mercury 2020.2.0 software was used for crystal structure analysis[35], preparation of crystal structure images and generation of full interaction maps[36] of FUR. FUR molecule conformation from different structures was overlaid in BIOVIA Discovery Studio Visualizer 4.5 by overlying the hydantoin ring atoms.

Theoretical calculations

Gas phase geometry optimization and calculation of conformer energy were performed in *Gaussian 09*[38] at M06-2X/6-31++G(d,p)//M06-2X/aug-cc-PVDZ level. Initial geometry of FUR molecule was taken from the crystal structure of FUR·THF·H_2O.

Geometry optimization of crystal structures was performed in Quantum ESPRESSO[39] by relaxing positions of all atoms. All calculations were performed using the PBE functional using ultra-soft pseudopotentials from the original pseudopotential library and a 44 Ry plane-wave cut-off energy with vdW interactions treated according to the D2 method of Grimme[40]. The selection of the pseudopotentials, parameters of convergence and the *k*-point grid were carried out using the published suggestions for structure optimizations of pharmaceutical molecules[41]. For FUR·DMSO II and FUR·DMSO III the disorder was removed and structures with the most probable solvent arrangement were used.

Pairwise intermolecular interaction energy calculations of crystal structures were performed in CrystalExplorer 17.5 at the B3LYP-D2/6-31G(d,p) level[42]. The sum over all pairwise interaction energies with molecules for which atoms are within 15 Å of the central molecule were used to estimate the lattice energy. Crystal structures were used after geometry optimization in Quantum ESPRESSO.

For calculation of interaction energy of FUR-solvent molecule pairs a molecule pair with the solvent molecule having an appropriate initial arrangement with reliable hydrogen bonding geometry was prepared and gas phase geometry optimization was performed in *Gaussian 09*[38] at M06-2X/6-31++G(d,p) level. More accurate energy was calculated at M06-2X/aug-cc-PVDZ level.

3. Results and discussion

3.1. Solvates obtained in the crystallization experiments

Crystallization of FUR from several solvents (DMF, DMA, DMSO, acetone, acetonitrile, nitromethane, ethyl acetate, THF, 1,4-dioxane, methyl tert-butyl ether, formic acid, acetic acid and water) showed that single solvent containing solvates can be obtained from solvents with different properties. Solvates were obtained with all three tested aprotic highly dipolar solvents DMF, DMA DMSO, with electron pair donor 1,4-dioxane and formic acid. Besides, in different crystallization experiments three different DMSO solvates were discovered. In addition, in crystallization from solvent and water mixtures a

number of solvate hydrates were obtained. Such solvates were obtained with part of the solvents forming the pure solvates (DMF, 1,4-dioxane and formic acid) and THF. Additionally, in one of the crystallization experiments from DMA/water a phase potentially being a DMA/water heterosolvate was obtained. The obtained solvates are listed in Table 2 and were characterized by thermal analysis (thermochemical data in Table 2, DSC/TG traces in Figures S3 and S4, Supporting Information) and by XRPD patterns (Figure 2).

Table 2. FUR solvates obtained in the crystallization experiments and their thermochemical data.

Solvent	Pure solvate	Weight loss / %	T_{des} / °C	Solvate hydrate	Weight loss / %	T_{des} / °C
DMF	FUR·DMF (1:1)	20.8 (*21.7*)[a]	115	FUR·DMF·H_2O (1:1:1)	25.1 (*25.6*)	60, 85
DMA	FUR·DMA (1:1)	23.8 (*24.8*)	125	(FUR·DMA·H_2O)[b] (1:1:1)	24.0 (*28.5*)	55, 115
	FUR·DMSO I (1:1)	21.9 (*22.8*)	140			
DMSO	FUR·DMSO II (1:1)	21.5 (*22.8*)	135	×		
	FUR·DMSO III (1:1)	21.8 (*22.8*)	135			
THF	×			FUR·THF·H_2O (1:1:1)	23.0 (*25.4*)	75
1,4-dioxane	FUR·DIOX (1:0.5)	14.2 (*14.3*)	140	FUR·DIOX·H_2O (1:0.5:1)	18.5 (*19.0*)	80, 110
Formic acid	FUR·FA (1:1)	14.1 (*14.8*)	100	FUR·FA·H_2O (1:1:1)	18.2 (*19.5*)	80

[a] – in parenthesis theoretical weight loss for the respective solvent stoichiometry is given

[b] – composition of the obtained phase is not crystallographically confirmed

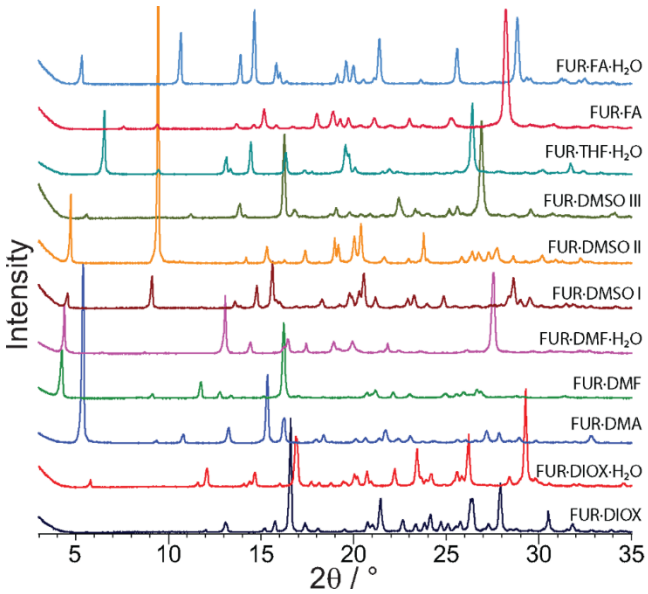

Figure 2. XRPD patterns of the FUR solvates and solvate hydrates.

For all of the solvates (except for the phase obtained from DMA/water) crystals suitable for SCXRD measurements were obtained and crystal structures were determined. The obtained crystallographic data are given in Table 1 and more details are available in Table S1. Although crystal structures of FUR THF·H_2O and FUR·DMF·H_2O were published as part of our previous study of FUR degradation[33], these structures are described and analysed here for the first time.

Most of the pure solvates has FUR : solvent ratio of 1:1. FUR·DMSO I and FUR·DMSO III crystallize in $P2_1/c$ space group and FUR·DMA crystallize in $Pca2_1$ space group, all containing 1 FUR and 1 solvent molecule in the asymmetric unit. FUR·DMSO II crystallize in $Pc2_1n$ space group containing 3 FUR and 3 solvent molecules in the asymmetric unit, FUR·DMF crystallize in $Pna2_1$ space group containing 4 FUR and 4 solvent molecules in the asymmetric unit and FUR·FA crystallize in *Pnma* space group containing 0.5 FUR molecules and a formic acid molecule on the mirror plane in the asymmetric unit. In contrast, FUR·DIOX has FUR : solvent ratio of 1 : 0.5 and is crystallizing in $P2_1/c$ space group containing 1 FUR and 0.5 solvent molecules in the asymmetric unit.

Most of the solvate hydrates has FUR : solvent : water ratio of 1 : 1 : 1. FUR·THF·H_2O and FUR·FA·H_2O crystallizing in $P\bar{1}$ space group and containing one molecule of each component in the asymmetric unit, whereas FUR·DMF·H_2O crystallizes in $P2_1/m$ space group and contains half molecule of each component in the asymmetric unit. FUR·DIOX·H_2O, however, has FUR : solvent : water ratio of 1 : 0.5 : 1 and is crystallizing in $P\bar{1}$ space group and contains 1 FUR, 1 water and 0.5 solvent molecules in the asymmetric unit.

In FUR·DMSO III the solvent molecule is disordered over two different arrangements with the same position for the oxygen atom and closely spaced sites for methyl groups (Figure S5). In FUR·DMSO II such disorder is present for one of the solvent molecules and in this case also the positions of the methyl groups are identical (Figure S5).

An overlay of the experimental and XRPD patterns simulated from the crystal structure data (see Figure S1) indicated that the crystal structures correspond to the bulk solid sample obtained in the crystallization. However, For FUR·DMA the crystal structure did not perfectly match the XRPD pattern of the bulk sample, with the perfectly matching peaks appearing in sample stored for 4 months (Figure S2).

The solvent stoichiometry as in the crystal structure was consistent with that determined for the bulk samples using TG analysis, see Table 2. We note that the desolvation of solvate hydrates always started at lower temperature than desolvation of the same solvent containing pure solvates. Part of the solvate hydrates desolvated in a single step (FUR·THF·H_2O and FUR·FA·H_2O). For FUR·DIOX·H_2O the first step appeared to be the loss of 1,4-dioxane, whereas the desolvation of FUR·DMF·H_2O appeared to be more complex multi-step process, see Figure S3. The analysis of the desolvation mechanism, however, was outside the scope of this study. The analysis of the product obtained in crystallization from DMA/water indicated that it corresponds to a solvate hydrate FUR·DMA·H_2O and the first desolvation step is the loss of water, but the lack of crystal structure of this phase makes this conclusion ambiguous.

3.2. Molecular conformation

FUR contains two flexible torsion angles τ_1 (O3-C4-C5-C6) and τ_2 (C7-N2-N3-C10) for each of which there are two energetically efficient geometries corresponding to 0° and 180°. In the crystal structures two of the potential conformers are observed: conformer A with torsion angle τ_1 being ~0° and τ_2 ~180° and conformer B with torsion angles τ_1 and τ_2 both being ~180°, see Figure 1. The gas phase energy difference between both conformers is 2 kJ mol^{-1} with conformer A calculated to be slightly more stable (Table S3). There are no crystal structures where τ_2 would be 0° even though the gas phase energy of such conformers is up to 8-10 kJ mol^{-1} more efficient. This conformer is still energetically favored in weakly polar solvents, while A and B are favored in polar solvents, see Table S3. One of the potential explanations for this could be that the intramolecular interaction C7-H···O4 present in conformer in which τ_2 is 0° reduces its energy but prevents as efficient intramolecular interactions as could be formed by conformer in which τ_2 is 180°.

In the studied solvates FUR molecule adopt different conformation. The three structurally similar solvate hydrates FUR·DIOX·H_2O, FUR·DMF·H_2O and FUR·THF·H_2O, two of the DMSO solvates FUR·DMSO I and FUR·DMSO II as well as the formic acid solvate FUR·FA contain conformer A. In contrast, most of the pure solvates FUR·DIOX, FUR·DMF, FUR·DMA, FUR·DMSO III and the remaining solvate hydrate FUR·FA·H_2O contain conformer B. Thus, except for the DMSO and formic acid solvates, in pure solvates conformer B is present, whereas in solvate hydrates it is the conformer A. Overlay of the FUR conformation in its solvates and solvate hydrates presented in Figure 3 show only small conformation adjustments for conformers A and B in different structures. The reported FUR polymorphs also contain both of these conformers: I contain conformer B, whereas II contain conformer A[32].

The conformation adopted by FUR results the molecule being almost planar, and the plane of the furan ring is nearly parallel to that of the hydantoin ring in most of the structures (angle between the planes is ≤5° for most of the solvates and 7.5° for FUR·DIOX·H_2O). However, the planes are somewhat twisted in FUR·DMA (16°) and FUR·DMSO II (27, 23 and 8° for each of the symmetrically unique molecule). This can be seen in Figure 3, as the most different are the molecules deviating from the planar conformation.

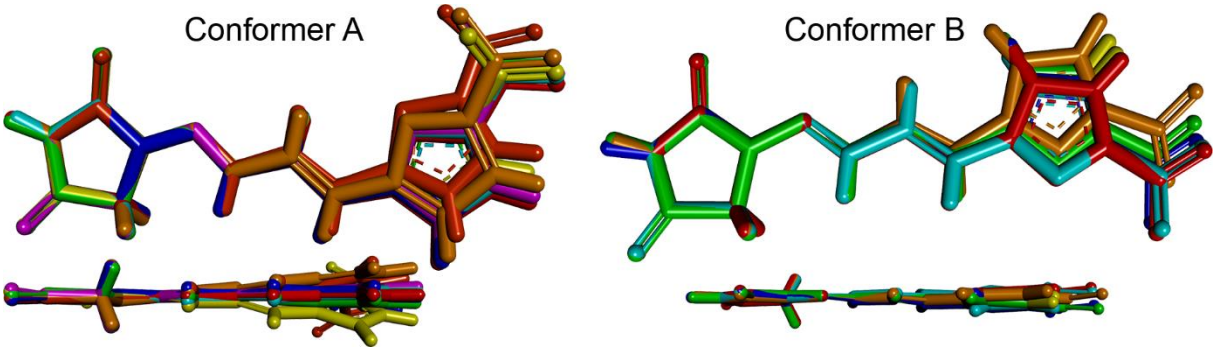

Figure 3. An overlay of FUR molecules in FUR solvates and solvate hydrates adopting a) conformation A (FUR·DIOX·H_2O blue, FUR·DMF·H_2O red, FUR·FA green, FUR·THF·H_2O cyan, FUR·DMSO I purple and FUR·DMSO II dark orange, light orange and yellow) and b) conformation B (FUR·DIOX blue, FUR·DMF red, FUR·FA·H_2O green, FUR·DMA cyan and FUR·DMSO III light orange). All symmetry independent molecules in FUR·DMA adopt identical conformation, see Figure S6.

3.3. **Hydrogen bonding and their energy**

As all of the organic solvents forming FUR solvates are able to participate in formation of strong hydrogen bond as hydrogen bond acceptors, not surprisingly, a hydrogen bond between FUR and solvent is present in crystal structures of nearly all FUR solvates. In all pure solvates except for the FUR·FA the only strong hydrogen bond therefore is N4-H···O_{Solv}, see Figure 4. In FUR·DMSO II and FUR·DMF this interaction is formed in each pair of symmetry independent FUR and solvent molecules.

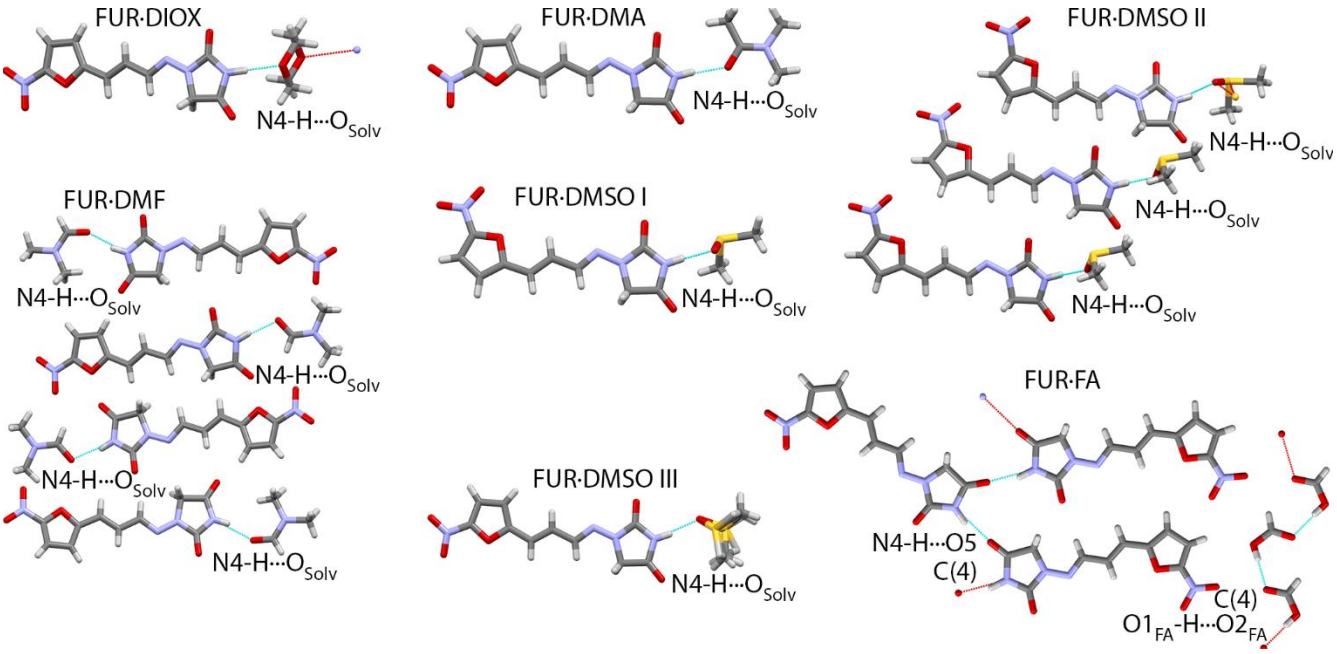

Figure 4. Hydrogen bonds observed in FUR solvates by showing the graph set notation of the hydrogen bond chains. Hydrogen bond geometry information is provided in Table S2.

Incorporation of water in the crystal structure allow formation of additional hydrogen bonds and apparently allow more efficient hydrogen bond network. In all solvate hydrates except for the FUR·FA·H_2O water is the acceptor and donor in the hydrogen bonds with FUR. Interactions N4-H···O_W and O_W-H···O5 are present in these solvate hydrates, while the organic solvent molecules form hydrogen bonds with water O_W-H···O_{Solv}, see Figure 5. Therefore, water acts as linker by linking the FUR molecules, and additionally act as a hook for binding organic solvent molecule. Both FUR···water hydrogen bonds form hydrogen bond chains $C^2_2(6)$. Even though, in contrast to THF and DMF, 1,4-dioxane forms two hydrogen bonds, the hydrogen bonding network in FUR·DIOX·H_2O is highly similar to that in FUR·THF·H_2O and FUR·DMF·H_2O. 1,4-dioxane is linked to two identical water molecules, and additional hydrogen bond chains $C^4_3(13)$ formed by all three hydrogen bonds are present in this structure, see Figure 5. Therefore, in this structure both solvent molecules act as linkers for FUR molecules.

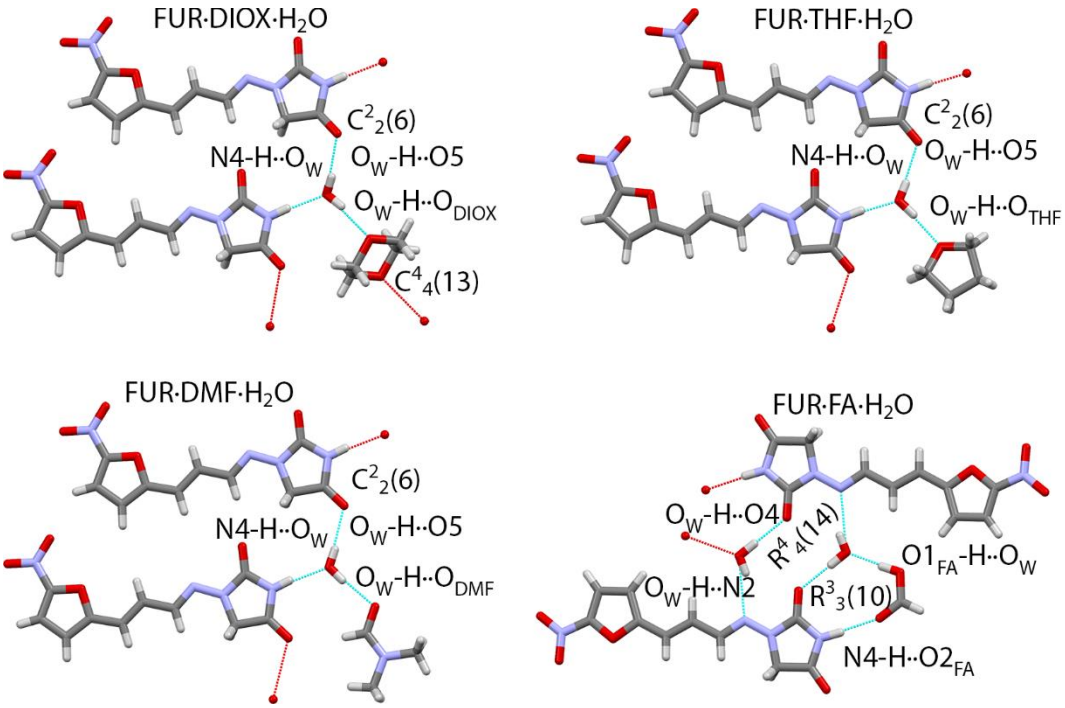

Figure 5. Hydrogen bonds observed in FUR solvate hydrates by showing the graph set notation of the hydrogen bond chains and rings. Hydrogen bond geometry information is provided in Table S2.

Compared to the other solvents forming solvates with FUR, formic acid is also a strong hydrogen bond donor which allows it to form notably different intermolecular interactions. Interestingly, in FUR·FA there are no hydrogen bonds between FUR and formic acid, see Figure 4. FUR forms hydrogen bond chains C(4) employing hydrogen bonds N4-H···O5, while formic acid molecules are situated next to the nitro groups of FUR and also forms hydrogen bond chains C(4) employing hydrogen bonds $O1_{FA}$-H···$O2_{FA}$, see Figure 5. Notably distinctive hydrogen bond network is also present in the solvate hydrate FUR·FA·H_2O, and in this solvate FUR is bonded to the formic acid by interaction N4-H···$O2_{FA}$. In

contrast to the other solvate hydrates, in this structure there is a FUR-water hydrogen bond formed by the other oxygen atom of the hydantoin ring O_W-H···O4 and water is a hydrogen bond donor in a second hydrogen bond with FUR O_W-H···N2. Water and formic acid are linked with hydrogen bond in which formic acid is the hydrogen bond donor $O1_{FA}$-H···O_W. Hydrogen bonds linking FUR, formic acid and water form hydrogen bond ring $R^3_3(10)$, while those linking two FUR and two water molecules form hydrogen bond ring $R^4_4(14)$.

It can be noted that in FUR·FA·H_2O atoms O4 and N2 act as the hydrogen bond acceptors of FUR molecule, while in the other solvate hydrates and FUR·FA it is atom O5. In all the other pure solvates none of the FUR atoms act as hydrogen bond acceptor. Based on the evaluation of the Full interaction maps (see Figure S7) no preference for O4 or O5 for involvement in the intermolecular interactions could be identified, while the location of hydrogen bond donor bonding with N2 partly overlapped with an alternative site able to bond also with O4.

The interaction energy between the hydrogen bonded molecules (formed by four energy components: electrostatic, polarization, dispersion, and exchange-repulsion) were calculated using CrystalExplorer 17.5 software and are given in Table 3. Although the used approach provides the overall interaction energy for the molecule pair, in all cases molecules are arranged so that the strong hydrogen bond is the only interaction of considerable importance. Thus, for simplicity, in the text the calculated interaction energy is attributed to the hydrogen bond energy.

The interaction N4-H···O_{Solv} is the strongest hydrogen bond in most of the solvates, with the energy for this interaction ranging from –40 to –53 kJ mol^{-1} in most of the cases, see Table 3. In contrast, in FUR·FA and FUR·FA·H_2O this interaction is –25 to –31 kJ mol^{-1}. As given above, in the remaining solvate hydrates FUR·DIOX·H_2O, FUR·DMF·H_2O and FUR·THF·H_2O this interaction is formed with water (N4-H···O_W). The energy of the other strong hydrogen bonds O_W-H···O_{Solv} and O_W-H···O5 in these structures range from –26 to –34 kJ mol^{-1}, see Table 3.

In comparison, in FUR·FA·H_2O the interaction energy for hydrogen bond N4-H···$O2_{FA}$ is less negative, while the energy of the other hydrogen bonds $O1_{FA}$-H···O_W, O_W-H···N2 and O_W-H···O4 range from –24 to –50 kJ mol^{-1}. The interaction $O1_{FA}$-H···O_W is notably stronger and O_W-H···N2 slightly stronger than any other hydrogen bond not involving N4-H, see Table 3. Meanwhile, in FUR·FA the rather weaker interaction N4-H···O5 is compensated by the interaction between the solvent molecules $O1_{FA}$-H···$O2_{FA}$ again being notably stronger than any other hydrogen bond not involving by N4-H.

Table 3. The pairwise interaction energy for the molecules forming strong hydrogen bonds in furazidin solvates. Electrostatic, polarization, dispersion, and exchange-repulsion energy components for each molecule pair are given in Tables S4 and S5.

Solvent	Phase	Interaction	E_{tot} / kJ mol^{-1}
1,4-dioxane	FUR·DIOX	N4-H···O_{DIOX}	-40.3
	FUR·DIOX·H_2O	N4-H···O_w	-44.4
		O_W-H···O_{DIOX}	-27.4
		O_W-H···O5	-25.7
DMF	FUR·DMF	N4A-H···O_{DMF1}	-49.9
		N4B-H···O_{DMF2}	-49.9
		N4C-H···O_{DMF3}	-42.5
		N4D-H···O_{DMF4}	-43.0
	FUR·DMF·H_2O	N4-H···O_w	-43.8
		O_W-H···O_{DMF}	-33.5
		O_W-H···O5	-27.6
THF	FUR·THF·H_2O	N4-H···O_w	-45.0
		O_W-H···O_{THF}	-28.4
		O_W-H···O5	-26.7
Formic acid	FUR·FA	N4-H···O5	-25.4
		$O1_{FA}$-H···$O2_{FA}$	-46.4
	FUR·FA·H_2O	N4-H···$O2_{FA}$	-31.2
		$O1_{FA}$-H···O_W	-49.5
		O_W-H···N2	-37.0
		O_W-H···O4	-24.2
DMA	FUR·DMA	N4-H···O_{DMA}	-52.9
DMSO	FUR·DMSO I	N4-H···O_{DMSO}	-45.0
	FUR·DMSO II	N4A-H···O_{DMSO1}	-39.6
		N4B-H···O_{DMSO2}	-45.1
		N4C-H···O_{DMSO3}	-46.0
	FUR·DMSO III	N4-H···O_{DMSO}	-46.5

In summary, when FUR solvate hydrates are formed by solvent able to act only as hydrogen bond acceptor, despite the different solvent properties, identical hydrogen bonds and their arrangement is present, and in all cases there is one hydrogen bond donor from the organic solvent in the asymmetric unit. In contrast, introduction of a hydrogen bond acceptor and donor solvent (formic acid) alters this hydrogen bond network and results a hydrogen bond pattern consisting of 4 hydrogen bonds. However, this only slightly increase the overall interaction energy resulting from the strong hydrogen bonds (from –98 to –105 for hydrogen bond acceptor solvents to –111 for hydrogen bond acceptor and donor formic acid), see Table S6.

3.4. Molecular packing

The two different molecular conformations together with variation of hydrogen bods and weak intermolecular interactions result in different packing possibilities of FUR and solvent molecules which are employed in the FUR solvates. In all the solvate hydrates FUR molecules and solvent molecules are arranged in layers with molecules interacting by the strong hydrogen bonds, the weak hydrogen bonds and other weak interactions, and these layers then stack above each other by interacting primarily by aromatic interactions (see Figure 6). In FUR·DMF·H_2O and FUR·THF·H_2O these layers consist of parallelly arranged sheets of hydrogen bonded molecules. In these sheets FUR is stacked in head-to-tail orientation (see Figure 1) interacting by two weak hydrogen bonds C7-H···O4 and C2-H···O2 and linked by the hydrogen bond chain $C^2_2(6)$, see Table S7 for the interaction energy between these molecules. As 1,4-dioxane molecules form two hydrogen bonds, the packing in FUR·DIOX·H_2O is slightly different. In otherwise similar layers to those in FUR·DMF·H_2O and FUR·THF·H_2O two adjacent sheets are hydrogen bonded via 1,4-dioxane and oriented in opposite directions, and the layer is stepped (see Figure 6). However, within the sheet the molecule arrangement and interactions are identical to that in FUR·DMF·H_2O and FUR·THF·H_2O.

In FUR·FA·H_2O the layers consist of discrete hydrogen bonded six molecule hexamers formed by 2 head-to-head oriented FUR, 2 formic acid and 2 water molecules. The FUR molecules from two adjacent hexamers are oriented either in tail-to-tail or head-to-tail manner and are bonded by weak hydrogen bonds of C-H···O type.

Such packing result in organic solvent molecules being located in solvent channels which are separated in FUR·DIOX·H_2O and FUR·FA·H_2O and nearly form a 2D solvent molecule layers in FUR·DMF·H_2O and FUR·THF·H_2O, see Figure S8. In all of the solvate hydrates water is located in pockets adjacent to the channel of the organic solvent.

In contrast to the solvate hydrates, only in part of the pure solvates molecules are arranged in parallelly stacked layers, see Figure 7. Interestingly, the packing in FUR·FA is rather similar to that in FUR·DIOX·H_2O, as FUR molecules are arranged in sheets in head-to-tail orientation and adjacent sheets in a layer are pointed in opposite directions. In contrast, FUR molecules in such adjacent sheets are hydrogen bonded by C(4) chains (and also by weak hydrogen bonds C7-H···O4 and C2-H···O2, see Table S7). Between each two such sheets there is a sheet of formic acid molecules which are also hydrogen bonded by C(4) chains.

Also in FUR·DMSO I and FUR·DMSO III FUR molecules are arranged in nearly planar layers (Figure 7). In FUR·DMSO I all FUR molecules in the layer are stacked in head-to-tail orientation and interact by two weak hydrogen bonds C7-H···O4 and C2-H···O2, see Table S7. Between the two sheets of FUR molecules there are DMSO molecules forming a layer perpendicular to that of FUR molecule layers.

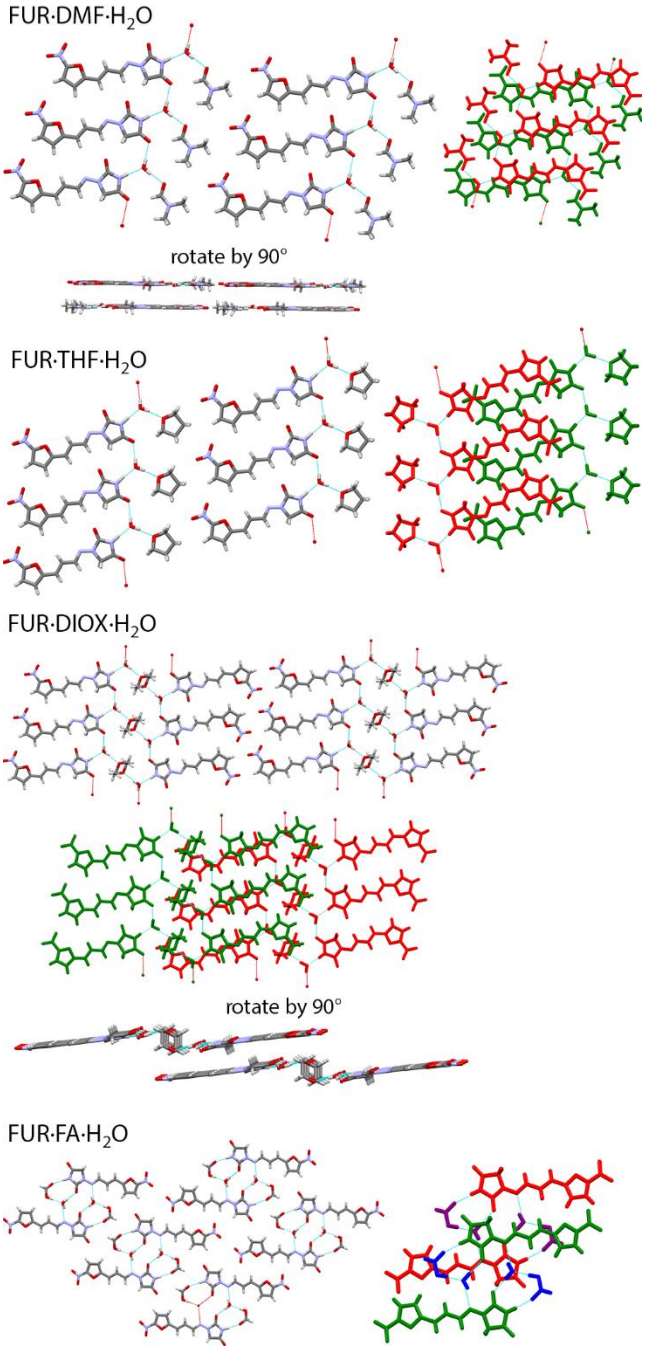

Figure 6. Molecular packing in FUR solvate hydrates. The most obvious layers of parallelly oriented FUR molecules are colored by elements. In the relative arrangement of such layers each layer is represented in different color. For selected structures the layers and their stacking are also demonstrated from a perpendicular perspective (designated by *rotate by 90°*).

In FUR·DMSO III the adjacent FUR molecules in the sheet are stacked in head-to-tail orientation. In contrast to the other structures, FUR molecules are oriented in opposite directions and therefore interact by different set of weak hydrogen bonds C7-H···O4, C6-H···O5 and C3-H···O5, see Table S7. Such

orientation leads to packing where the hydrogen bonded DMSO molecules are situated in isolated sites within the layer. Adjacent sheets of FUR molecules in a layer are pointed in opposite directions.

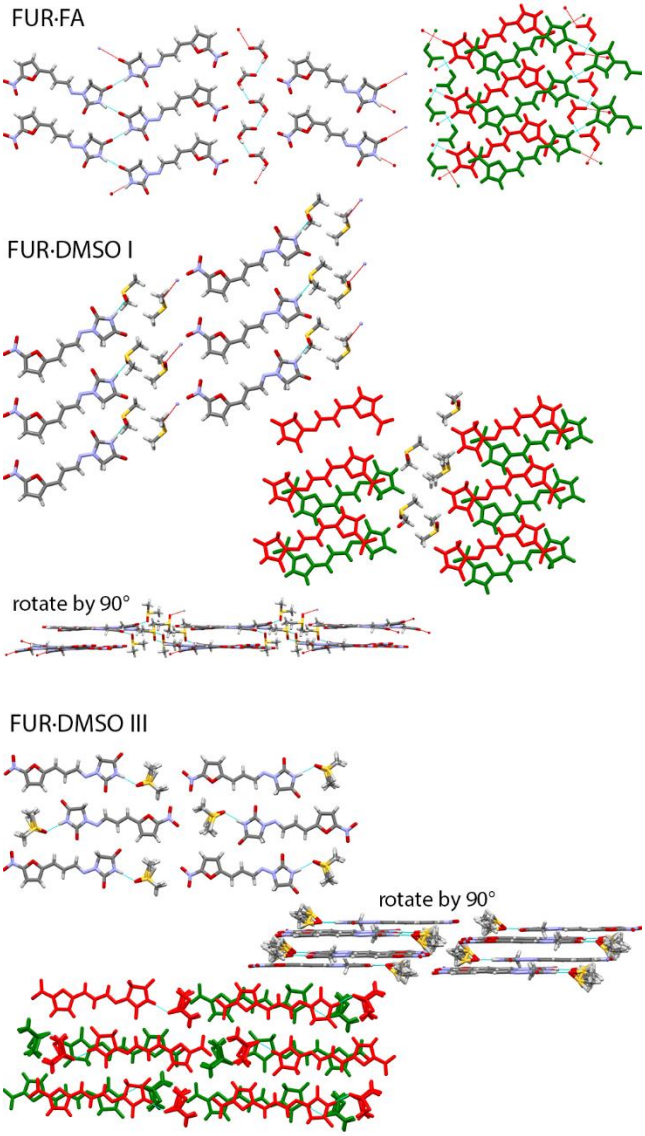

Figure 7. Molecular packing in FUR solvates formed by parallel layers consisting of sheets of FUR molecules connected by weak hydrogen bonds. The most obvious layers of parallelly oriented FUR molecules are colored by elements. In the relative arrangement of such layers each layer is represented in different color. For selected structures the layers and their stacking are also demonstrated from a perpendicular perspective (designated by *rotate by 90°*).

In most of the remaining pure solvates a layer of π··· π stacked FUR molecules can be identified as the main packing construct, see Figure 8. In FUR·DMA such layers of parallel π··· π stacked FUR molecules are infinite in 2D and has a width of one FUR molecule. In this layer each two adjacent FUR molecules are oriented in opposite directions. The resulting crystal structure is formed by stacking each two adjacent layers nearly perpendicular to each other by employing weak hydrogen bonds C-H···O

formed by O4 and O5 atoms, see Table S7. In FUR·DMF such layers of parallel π··· π stacked FUR molecules is infinite in 2D and has width of two molecules. In this layer each two adjacent FUR molecules are oriented in opposite directions. The resulting crystal structure is formed by stacking such layers by employing weak hydrogen bonds C-H···O formed by O4 and O5 atoms so that two adjacent layers are tilted with respect to each other. In FUR·DIOX such layers of parallel π··· π stacked FUR molecules are infinite in 2D and has width of one FUR molecule. In this layer each two adjacent FUR molecules are oriented in opposite directions, and dioxane hydrogen bonds two FUR molecules from adjacent sheets within a layer. The resulting crystal structure is formed by stacking such layers by employing weak hydrogen bonds C-H···O formed by O4, O5 and O2 atoms so that two adjacent layers are tilted with respect to each other.

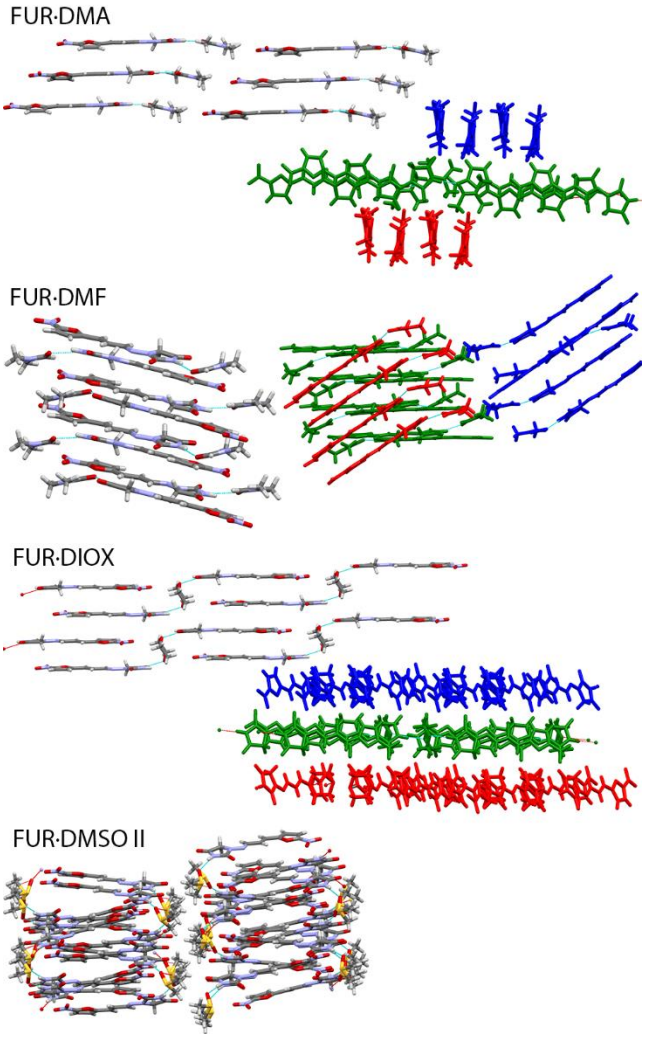

Figure 8. Molecular packing in FUR solvates formed by layers consisting of sheets of parallel π···π stacked FUR molecules and in FUR·DMSO II. The most obvious layers of parallelly oriented FUR molecules are colored by elements. In the relative arrangement of such layers each layer is represented in different color.

In FUR·DMSO II, however, no construct of parallel FUR molecules could be identified, and the overall crystal structure could be described as consisting of 2D layers of FUR molecules oriented in different directions and separated by layers of DMSO molecules. FUR molecules within such layer interact by both weak hydrogen bonds C-H···O formed by O4 and O2 and by π··· π interactions, see Table S7.

The packing of pure solvates resulted in clear solvent molecule layers being present in FUR·DMSO I and FUR·DMSO II and clear channels being present in FUR·FA, see Figure S8. Despite the different arrangement of FUR molecules, nearly identical identically located disrupted solvent layers formed by clear solvent channels are present in FUR·DMSO III and FUR·DMA, and similar disrupted solvent layers formed by clear solvent channels are present in FUR·DMF. The lower solvent stoichiometry in FUR·DIOX resulted this structure to be the only one in which solvent is located in isolated pockets.

3.5. Furazidin-solvent interaction strength

Additional to the interaction energy in the observed crystal structures also interaction energy for isolated dimers were calculated. Several possible hydrogen bonds were probed for water and formic acid (for the latter the data of only the most stable dimers are shown). The results show that the strongest hydrogen bond by N4-H is formed by the strongest hydrogen bond acceptors DMSO, DMF and DMA ($\Delta E < -50$ kJ mol^{-1}). Nevertheless, the strongest interaction is formed by the only hydrogen bond acceptor and donor formic acid ($\Delta E = -65$ kJ mol^{-1}, resulting from two interactions N4-H···O2$_{FA}$ and O1$_{FA}$-H···O4), see Table 4. In contrast, interaction of 1,4-dioxane, THF and water with N4-H are no stronger than –45 kJ mol^{-1}, even though water in these dimers additionally form hydrogen bond with O4 or N2 atoms. Interactions where water is hydrogen bond donor and N2 or O5 atoms of FUR are hydrogen bond acceptors are even less efficient ($\Delta E < -40$ kJ mol^{-1}). As expected, the FUR conformation had very small effect on the stability of the dimers, as the atoms involved in formation of the strong hydrogen bonds are not affected.

Table 4. Interaction energy (in kJ mol^{-1}) for FUR dimers with selected solvents (with FUR in conformation A and B) identifying the interaction(s) present and solvate(s) where such dimer is present.

Dimer	Interaction[a]	Present in	ΔE / kJ mol^{-1}
Fur-DIOX (A)	$_{A}$N4-H···O$_{DIOX}$	–	-41.5
Fur-DIOX (B)	$_{B}$N4-H···O$_{DIOX}$	FUR·DIOX[b]	-41.1
Fur-THF (A)	$_{A}$N4-H···O$_{THF}$	–	-44.6
Fur-THF (B)	$_{B}$N4-H···O$_{THF}$	–	-44.1
Fur-DMA (A)	$_{A}$N4-H···O$_{DMA}$	–	-51.4
Fur-DMA (B)	$_{B}$N4-H···O$_{DMA}$	FUR·DMA[b]	-51.5
Fur-DMF (A)	$_{A}$N4-H···O$_{DMF}$	–	-52.9
Fur-DMF (B)	$_{B}$N4-H···O$_{DMF}$	FUR·DMF[b]	-52.2
Fur-DMSO (A)	$_{A}$N4-H···O$_{DMSO}$	FUR·DMSO I, FUR·DMSO II[b]	-58.9
Fur-DMSO (B)	$_{B}$N4-H···O$_{DMSO}$	FUR·DMSO III[b]	-60.3
Fur-H2O-1 (A)	$_{A}$N4-H···O$_{W}$ + O$_{W}$-H···$_{A}$O5	(FUR·DIOX·H_2O, FUR·DIMF·H_2O, FUR·THF·H_2O)[c]	-41.9
Fur-H2O-1 (B)	$_{B}$N4-H···O$_{W}$ + O$_{W}$-H···$_{B}$O5		-42.3
Fur-H2O-2 (A)	O$_{W}$-H···$_{A}$O5	(FUR·DIOX·H_2O, FUR·DIMF·H_2O, FUR·THF·H_2O)[c]	-36.5
Fur-H2O-2 (B)	O$_{W}$-H···$_{B}$O5		-36.4
Fur-H2O-3 (A)	$_{A}$N4-H···O$_{W}$ + O$_{W}$-H···$_{A}$O4		-44.7
Fur-H2O-3 (B)	$_{B}$N4-H···O$_{W}$ + O$_{W}$-H···$_{B}$O4		-44.3
Fur-H2O-4 (A)	O$_{W}$-H···$_{A}$N2	(FUR·FA·H_2O)[c]	-31.4
Fur-H2O-4 (B)	O$_{W}$-H···$_{B}$N2		-38.0
Fur-FA (A)	$_{A}$N4-H···O2$_{FA}$ + O1$_{FA}$-H···$_{A}$O4	–	-65.4
Fur-FA (B)	$_{B}$N4-H···O2$_{FA}$ + O1$_{FA}$-H···$_{B}$O4	(FUR·FA·H_2O)[d]	-65.0

[a] – The lower index A and B before the O/N atom of FUR denotes the conformer A or B.

[b] – in the crystal structure geometry of dimer is somewhat different, as weak hydrogen bond formed by FUR O4 or O5 atoms and solvent hydrogens are not always identical.

[c] – in the crystal structure geometry of dimer is different, as water just forms the strong hydrogen bond $_{A}$N4-H···O$_{W}$, O$_{W}$-H···$_{A}$O5 or O$_{W}$-H···$_{A}$N2 and is arranged further apart from other FUR atoms.

[d] – in the crystal structure geometry of dimer is different, as formic acid just forms the strong hydrogen bond $_{B}$N4-H···O2$_{FA}$ and is arranged further apart from other FUR atoms.

3.6. Solvate formation of furazidin

In FUR solvates with hydrogen bond acceptor solvents hydrogen bond N4-H···O$_{Solv}$ is always present. In these solvates FUR molecules interact with each other mainly by π··· π stacking in mostly approximately perpendicular direction and also by weak hydrogen bonds formed by the carboxyl group or the nitro group oxygen atoms in approximately planar direction. Such hydrogen bonding is rather

typical for molecules having only one hydrogen bond donor site and forming solvates with hydrogen bond acceptor solvents, and observed also for structurally similar nitrofurantoin[43-44] and several benzoic acid derivatives[45].

As this is the only strong hydrogen bond in pure solvates such solvates can be obtained only with good hydrogen bond acceptors, as the interaction N4-H···O_{Solv} has to be efficient enough. Considering the hydrogen bond acceptor propensity β[46] of the solvents used in this study, it can be confirmed that this is highly important factor determining the solvate formation, as solvates are obtained almost exclusively with the solvents having the largest β values, see Table 5.

Table 5. Solvent hydrogen bond acceptor propensity (β) for the solvents used in this study together with the obtained solvates.

Solvent	β	Pure solvate	Solvate hydrate
DMSO	0.88	✓	×
DMA	0.78	✓	(✓)
DMF	0.74	✓	✓
1,4-dioxane	0.64	✓	✓
acetone	0.49	×	×
THF	0.48	×	✓
Water	0.47	×	×
Ethyl acetate	0.45	×	×
Acetic acid	0.44	×	×
Methyl tert-butyl ether	0.40	×	×
Formic acid	0.38	✓	✓
Acetonitrile	0.32	×	×
Nitromethane	0.31	×	×

As described, incorporation of water molecules provides additional possibilities for hydrogen bonding. The calculated lattice energy shows that the hydrogen bonding network in the solvate hydrates is more efficient than that in the pure solvates, and incorporation of water lower the lattice energy by 60.5 to 68.6 kJ/mol (calculated per FUR molecule, see Table S9). With the hydrogen bond acceptor solvents the most efficient packing apparently is in a structure in which water molecules link FUR molecules by forming infinite chains, while solvent molecules are bound (or "hooked") to the water molecules, with the dioxane bound to two such chains. Such hydrogen bonding is similar to that in the only reported solvate hydrate[44] and one of the co-crystal hydrates[47] of structurally similar nitrofurantoin and solvate hydrates of 3,5-dihydroxybenzoic acid[16]. Because of this linkage the hydrogen bond acceptor propensity β of the solvents is also the factor determining the solvent selection for formation of solvate hydrates. However, not all the potential solvate hydrates are obtained (e.g., containing DMSO), whereas a solvate hydrate with THF is obtained even though THF is not as efficient hydrogen bond acceptor solvent as the other solvate forming solvents (except for the formic acid).

The interaction energies in solvate crystal structures (Table 3) and isolated dimers (Table 4) do not explain the absence of a DMSO solvate hydrate. As described above, FUR and water in all the experimentally obtained solvate hydrates form hydrogen bonded sheets stacking in planar or nearly planar layers. It can be speculated that the absence of DMSO solvate hydrate could be explained by the ability of DMSO to form very stable pure solvate structures where FUR molecules form planar arrangement (FUR·DMSO I and FUR·DMSO III). Alternatively, this could be because of the inability of DMSO to provide a stable solvate hydrate structure with planar arrangement of hydrogen bonding network.

The formation of THF solvate hydrate could be explained by the fact that in solvate hydrates with the hydrogen bond acceptor solvents the only hydrogen bond formed by the organic solvent is O_W-H···O_{Solv}. This is weaker interaction than N4-H···O_{Solv} present in pure solvates and, moreover, is just part of the strong hydrogen bond network present in these solvates. Therefore, it is not surprising that solvate hydrates could be obtained with solvents having lower hydrogen bond acceptor propensity β.

As formic acid is not only the hydrogen bond acceptor but also a rather strong hydrogen bond donor, formation of additional hydrogen bonds is possible, which therefore explain the existence of formic acid solvates FUR·FA and FUR·FA·H_2O despite its relatively low hydrogen bond acceptor propensity β. Interestingly, in FUR·FA apparently the most efficient packing is achieved by FUR and formic acid forming hydrogen bonds among themselves, therefore two separate hydrogen bond chains formed by each of the two components are present. These differences also result in FUR·FA·H_2O being different from the rest of the solvate hydrates, as in this structure solvent molecules are directly linked to the FUR and also to the water, while two water molecules link two FUR molecules using FUR hydrogen bond acceptor sites O4 and N2. Although O4 is not involved in hydrogen bonding in any other solvate structure, both hydantoin ring oxygen atoms O4 and O5 have similar propensity to form hydrogen bonds. This is demonstrated by the evaluation of the Full interaction maps (see Figure S7) and both atoms are used in hydrogen bonds formed in the crystal structures of FUR polymorphs[32].

Nevertheless, it should be kept in mind that there are numerous aspects which determine the solvate formation, and characterization of many of these is either nearly impossible or very complicated (e.g., thermodynamic stability, its temperature dependence, nucleation kinetics, solubility aspects etc.) and therefore outside the scope of this study. Therefore, it is not surprising that solvate formation cannot be explained based purely on the solvent hydrogen bond acceptor propensity β. For example, this criterion does not allow to explain why solvates with similar β values to THF (acetone, ethyl acetate) does not form solvate hydrates. Among additional factors the solvent size and shape can be highlighted in this case, as only solvates for which energetically efficient molecular packing can be achieved will be obtained[48-50].

CONCLUSIONS

In summary, we have obtained and characterized multiple furazidin solvates and solvate hydrates. FUR forms solvates with solvents having large hydrogen bond acceptor propensity β, and this is confirmed by formation of three DMSO solvates, DMA, DMF and 1,4-dioxane solvates. In all of these solvates the only hydrogen bond present is N4-H···O_{Solv}. An additional solvate is obtained with a hydrogen bond donor and acceptor formic acid, and in this solvate FUR and formic acid molecules each form separate hydrogen bond chains. Crystal structure of all solvates can be described as formed from layers, and in DMA, DMF and 1,4-dioxane solvates these are layers of π··· π stacked FUR molecules which are packed in different orientation with respect to each other. In formic acid solvate these are planes containing the hydrogen bonded molecule chains. In two of the DMSO solvates these are planar or nearly planar planes formed from the hydrogen bonded FUR-DMSO dimers, whereas in the third DMSO solvate these are layers of FUR molecules oriented in different directions.

In FUR solvate hydrates the incorporation of water allows formation of additional hydrogen bonds and results in more efficient hydrogen bond network. In solvate hydrates formed by hydrogen bond acceptor solvents water forms three hydrogen bonds by linking the FUR molecules via interactions N4-H···O_W and O_W-H···O5 and also "hooks" the organic solvent molecule via interaction O_W-H···O_{Solv}. Also in FUR solvate hydrates hydrogen bond acceptor propensity of the solvent is highly important, although the lower importance of the hydrogen bond formed by the solvent allows formation of solvate hydrates not only with the very good hydrogen bond acceptors DMF and 1,4-dioxane but also with THF. A solvate hydrate was obtained also with formic acid, but the additional hydrogen bond donor of this solvent results in changed hydrogen bond network with relatively lower importance of the hydrogen bonds formed by the water. Clear layers are present in all of the solvate hydrates, with layers formed by sheets of hydrogen bonded entities in DMF, 1,4-dioxane, and THF solvate hydrates, and by hydrogen bonded hexamers in formic acid solvate hydrate.

ASSOCIATED CONTENT

Supporting Information. The Supporting Information is available free of charge at https://pubs.acs.org/doi/10.1021/
Detailed and additional information on furazidin solvate and solvate hydrate characterization, crystal structure determination and analysis. (PDF)

AUTHOR INFORMATION

Corresponding Author
*Telephone: +(371)-67033903. E-mail: agris.berzins@lu.lv.

Funding Sources

This work has been supported by the Latvian Council of Science, project "Crystal engineering of pharmaceutical multicomponent phases for more efficient crystalline phase design", project No. lzp-2018/1-0312.

Notes

The authors declare no competing financial interest.

REFERENCES

1. Stahly, G. P. Diversity in Single- and Multiple-Component Crystals. The Search for and Prevalence of Polymorphs and Cocrystals. *Cryst. Growth Des.* 2007, *7* (6), 1007-1026.
2. Hilfiker, R.; Von Raumer, M. *Polymorphism in the Pharmaceutical Industry: Solid Form and Drug Development*. John Wiley & Sons: Weinheim, 2018; p 469.
3. Cruz-Cabeza, A. J.; Reutzel-Edens, S. M.; Bernstein, J. Facts and fictions about polymorphism. *Chem. Soc. Rev.* 2015, *44* (23), 8619-8635.
4. Bryant, M. J.; Black, S. N.; Blade, H.; Docherty, R.; Maloney, A. G. P.; Taylor, S. C. The CSD Drug Subset: The Changing Chemistry and Crystallography of Small Molecule Pharmaceuticals. *J. Pharm. Sci.* 2019, *108* (5), 1655-1662.
5. Li, Y.; Yu, H.; Xu, F.; Guo, Q.; Xie, Z.; Sun, Z. Solvent controlled self-assembly of π-stacked/H-bonded supramolecular organic frameworks from a C3-symmetric monomer for iodine adsorption. *CrystEngComm* 2019, *21* (11), 1742-1749.
6. Kazuaki, H. The Structure of the Cyclodextrin Complex. VII. The Crystal Structure of the α-Cyclodextrin–DMSO–Methanol(1 : 1 : 2) Dihydrate Complex A Simultaneous Inclusion of DMSO and Methanol. *Bull. Chem. Soc. Jpn.* 1978, *51* (6), 1644-1648.
7. Huc, I.; Maurizot, V.; Gornitzka, H.; Léger, J.-M. Hydroxy-substituted oligopyridine dicarboxamide helical foldamers. *Chem. Commun.* 2002, (6), 578-579.
8. Berl, V.; Huc, I.; Khoury, R. G.; Lehn, J.-M. Helical Molecular Programming: Folding of Oligopyridine-dicarboxamides into Molecular Single Helices. *Chem. Eur. J.* 2001, *7* (13), 2798-2809.
9. Takieddin, K.; Khimyak, Y. Z.; Fábián, L. Prediction of Hydrate and Solvate Formation Using Statistical Models. *Cryst. Growth Des.* 2016, *16* (1), 70-81.
10. Price, C. P.; Glick, G. D.; Matzger, A. J. Dissecting the Behavior of a Promiscuous Solvate Former. *Angew. Chem., Int. Ed.* 2006, *45* (13), 2062-2066.
11. Vippagunta, S. R.; Brittain, H. G.; Grant, D. J. W. Crystalline solids. *Adv. Drug Delivery Rev.* 2001, *48*, 3-26.
12. Tessler, L.; Goldberg, I. Crystal Structures of Aripiprazole, a New Anti-psychotic Drug, and of its Inclusion Compounds with Methanol, Ethanol and Water. *J. Inclusion Phenom. Macrocyclic Chem.* 2006, *55* (3-4), 255-261.
13. Bhardwaj, R. M.; Price, L. S.; Price, S. L.; Reutzel-Edens, S. M.; Miller, G. J.; Oswald, I. D. H.; Johnston, B. F.; Florence, A. J. Exploring the Experimental and Computed Crystal Energy Landscape of Olanzapine. *Cryst. Growth Des.* 2013, *13* (4), 1602-1617.
14. Tieger, E.; Kiss, V.; Pokol, G.; Finta, Z.; Rohlíček, J.; Skořepová, E.; Dušek, M. Rationalization of the formation and stability of bosutinib solvated forms. *CrystEngComm* 2016, *18* (48), 9260-9274.
15. Karpinska, J.; Erxleben, A.; McArdle, P. 17β-Hydroxy-17α-methylandrostano[3,2-c]pyrazole, Stanozolol: The Crystal Structures of Polymorphs 1 and 2 and 10 Solvates. *Cryst. Growth Des.* 2011, *11* (7), 2829-2838.
16. Varughese, S.; Desiraju, G. R. Using Water as a Design Element in Crystal Engineering. Host–Guest Compounds of Hydrated 3,5-Dihydroxybenzoic Acid. *Cryst. Growth Des.* 2010, *10* (9), 4184-4196.
17. Trimdale, A.; Mishnev, A.; Bērziņš, A. Combined Use of Structure Analysis, Studies of Molecular Association in Solution, and Molecular Modelling to Understand the Different Propensities of Dihydroxybenzoic Acids to Form Solid Phases. *Pharmaceutics* 2021, *13* (5), 734.

18. Caira, M. R.; Nassimbeni, L. R.; Scott, J. L. Crystal structure and multiphase decomposition of a novel cholic acid inclusion compound with mixed guests. *J. Chem. Soc. Perkin Trans. 2* 1994, (7), 1403-1405.
19. Shikii, K.; Sakamoto, S.; Seki, H.; Utsumi, H.; Yamaguchi, K. Narcissistic aggregation of steroid compounds in diluted solution elucidated by CSI-MS, PFG NMR and X-ray analysis. *Tetrahedron* 2004, *60* (15), 3487-3492.
20. Candeloro De Sanctis, S.; Coiro, V. M.; Giglio, E.; Pagliuca, S.; Pavel, N. V.; Quagliata, C. The hexagonal phase of the 3:2:1 canal complex between deoxycholic acid, ethanol and water: an inclusion compound with hydrophilic channels. *Acta Crystallogr., Sect. B* 1978, *34* (6), 1928-1933.
21. Candeloro De Sanctis, S.; Giglio, E.; Petri, F.; Quagliata, C. The 2:1:1 canal complex between deoxycholic acid, dimethyl sulphoxide and water. *Acta Crystallogr., Sect. B* 1979, *35* (1), 226-228.
22. Zhang, G.; Wang, N.; Shang, X.; Zhang, L.; Wang, R.; Zhang, S. Solvates of acotiamide hydrochloride: characterization and phase transformation. *Acta Crystallogr., Sect. B* 2019, *75* (6), 1106-1114.
23. Behbehani, H.; Dawood, K. M.; Ibrahim, H. M.; Mostafa, N. S. Regio- and stereoselective route to bis-[3-methyl-1,1′,4′-triaryl-5-oxo-spiro-pyrazoline-4,5′-pyrazoline] derivatives via 1,3-dipolar cycloaddition under sonication. *Arab. J. Chem.* 2018, *11* (7), 1053-1060.
24. Berl, V.; Schmutz, M.; Krische, M. J.; Khoury, R. G.; Lehn, J.-M. Supramolecular Polymers Generated from Heterocomplementary Monomers Linked through Multiple Hydrogen-Bonding Arrays—Formation, Characterization, and Properties. *Chem. Eur. J.* 2002, *8* (5), 1227-1244.
25. Larsen, T. O.; Frydenvang, K.; Frisvad, J. C.; Christophersen, C. UV-Guided Isolation of Alantrypinone, a Novel Penicillium Alkaloid. *J. Nat. Prod.* 1998, *61* (9), 1154-1157.
26. Grinev, V. S.; Babkina, N. V.; Yegorova, A. Y. (E)-7-[(4-Nitrophenyl)diazenyl]-3a-(p-tolyl)-2,3,3a,4-tetrahydro-1H-benzo[d]pyrrolo[1,2-a]imidazol-1-one 0.58-dimethyl sulfoxide 0.42-acetonitrile solvate: crystal structure, Hirshfeld analysis and DFT estimation of the energy of intermolecular interactions. *Acta Crystallogr., Sect. E* 2017, *73* (10), 1590-1594.
27. Yang, J.; Rousselin, Y.; Bucher, L.; Desbois, N.; Bolze, F.; Xu, H.-J.; Gros, C. P. Two-Photon Absorption Properties and Structures of BODIPY and Its Dyad, Triad and Tetrad. *ChemPlusChem* 2018, *83* (9), 838-844.
28. Gillon, A. L.; Feeder, N.; Davey, R. J.; Storey, R. Hydration in Molecular CrystalsA Cambridge Structural Database Analysis. *Cryst. Growth Des.* 2003, *3* (5), 663-673.
29. Schwan, T. J.; Ebetino, F. H. Antibacterial Agents, Nitrofurans. In *Kirk-Othmer Encyclopedia of Chemical Technology*. John Wiley & Sons, 2000, DOI: 10.1002/0471238961.
30. Slapšyte, G.; Jankauskiene, A.; Mierauskiene, J.; Lazutka, J. R. Cytogenetic analysis of children under long-term antibacterial therapy with nitroheterocyclic compound furagin. *Mutat. Res.* 2001, *491* (1), 25-30.
31. Liepins, V.; Skomorokhov, M.; Lukjanova, N.; Matiushenkov, E.; Revjuka, J. Polymorphic forms of furazidin. Patent No. WO 2015/181741A1. 2015.
32. Dudek, M. K.; Paluch, P.; Pindelska, E. Crystal structures of two furazidin polymorphs revealed by a joint effort of crystal structure prediction and NMR crystallography. *Acta Crystallogr., Sect. B* 2020, *76* (3), 322-335.
33. Bērziņš, K.; Kons, A.; Grante, I.; Dzabijeva, D.; Nakurte, I.; Actiņš, A. Multi-technique approach for qualitative and quantitative characterization of furazidin degradation kinetics under alkaline conditions. *J. Pharm. Biomed. Anal.* 2016, *129*, 433-440.
34. Sheldrick, G. Crystal structure refinement with SHELXL. *Acta Crystallogr., Sect. C* 2015, *71* (1), 3-8.
35. Macrae, C. F.; Sovago, I.; Cottrell, S. J.; Galek, P. T. A.; McCabe, P.; Pidcock, E.; Platings, M.; Shields, G. P.; Stevens, J. S.; Towler, M.; Wood, P. A. Mercury 4.0: from visualization to analysis, design and prediction. *J. Appl. Crystallogr.* 2020, *53* (1), 226-235.
36. Wood, P. A.; Olsson, T. S. G.; Cole, J. C.; Cottrell, S. J.; Feeder, N.; Galek, P. T. A.; Groom, C. R.; Pidcock, E. Evaluation of molecular crystal structures using Full Interaction Maps. *CrystEngComm* 2013, *15* (1), 65-72.
37. Spek, A. L. Structure validation in chemical crystallography. *Acta Crystallogr., Sect. D* 2009, *65* (2), 148-155.
38. Frisch, M. J.; Trucks, G. W.; Schlegel, H. B.; Scuseria, G. E.; Robb, M. A.; Cheeseman, J. R.; Scalmani, G.; Barone, V.; Mennucci, B.; Petersson, G. A.; Nakatsuji, H.; Caricato, M.; Li, X.; Hratchian, H. P.; Izmaylov, A. F.; Bloino, J.; Zheng, G.; Sonnenberg, J. L.; Hada, M.; Ehara, M.; Toyota, K.; Fukuda, R.; Hasegawa, J.;

Ishida, M.; Nakajima, T.; Honda, Y.; Kitao, O.; Nakai, H.; Vreven, T.; Montgomery, J. A. J.; Peralta, J. E.; Ogliaro, F.; Bearpark, M.; Heyd, J. J.; Brothers, E.; Kudin, K. N.; Staroverov, V. N.; Kobayashi, R.; Normand, J.; Raghavachari, K.; Rendell, A.; Burant, J. C.; Iyengar, S. S.; Tomasi, J.; Cossi, M.; Rega, N.; Millam, J. M.; Klene, M.; Knox, J. E.; Cross, J. B.; Bakken, V.; Adamo, C.; Jaramillo, J.; Gomperts, R.; Stratmann, R. E.; Yazyev, O.; Austin, A. J.; Cammi, R.; Pomelli, C.; Ochterski, J. W.; Martin, R. L.; Morokuma, K.; Zakrzewski, V. G.; Voth, G. A.; Salvador, P.; Dannenberg, J. J.; Dapprich, S.; Daniels, A. D.; Farkas, O.; Foresman, J. B.; Ortiz, J. V.; Cioslowski, J.; Fox, D. J. *Gaussian 09, Revision D.01*; Gaussian Inc.: Wallingford, CT, 2009.

39. Giannozzi, P.; Baroni, S.; Bonini, N.; Calandra, M.; Car, R.; Cavazzoni, C.; Ceresoli, D.; Chiarotti, G. L.; Cococcioni, M.; Dabo, I.; Dal Corso, A.; de Gironcoli, S.; Fabris, S.; Fratesi, G.; Gebauer, R.; Gerstmann, U.; Gougoussis, C.; Kokalj, A.; Lazzeri, M.; Martin-Samos, L.; Marzari, N.; Mauri, F.; Mazzarello, R.; Paolini, S.; Pasquarello, A.; Paulatto, L.; Sbraccia, C.; Scandolo, S.; Sclauzero, G.; Seitsonen, A. P.; Smogunov, A.; Umari, P.; Wentzcovitch, R. M. QUANTUM ESPRESSO: a modular and open-source software project for quantum simulations of materials. *J. Phys.: Condens. Matter* 2009, *21* (39), 395502.

40. Grimme, S. Semiempirical GGA-type density functional constructed with a long-range dispersion correction. *J. Comput. Chem.* 2006, *27* (15), 1787-1799.

41. Lund, A. M.; Orendt, A. M.; Pagola, G. I.; Ferraro, M. B.; Facelli, J. C. Optimization of Crystal Structures of Archetypical Pharmaceutical Compounds: A Plane-Wave DFT-D Study Using Quantum Espresso. *Cryst. Growth Des.* 2013, *13* (5), 2181-2189.

42. Mackenzie, C. F.; Spackman, P. R.; Jayatilaka, D.; Spackman, M. A. CrystalExplorer model energies and energy frameworks: extension to metal coordination compounds, organic salts, solvates and open-shell systems. *IUCrJ* 2017, *4* (5), 575-587.

43. Tutughamiarso, M.; Bolte, M.; Wagner, G.; Egert, E. Five pseudopolymorphs and a cocrystal of nitrofurantoin. *Acta Crystallogr., Sect. C* 2011, *67* (1), o18-o25.

44. Vangala, V. R.; Chow, P. S.; Tan, R. B. H. The solvates and salt of antibiotic agent, nitrofurantoin: structural, thermochemical and desolvation studies. *CrystEngComm* 2013, *15* (5), 878-889.

45. Bērziņš, A.; Kons, A.; Saršūs, K.; Belyakov, S.; Actiņš, A. On the Rationalization of Formation of Solvates: Experimental and Computational Study of Solid Forms of Several Nitrobenzoic Acid Derivatives. *Cryst. Growth Des.* 2020, *20* (9), 5767-5784.

46. Gu, C.-H.; Li, H.; Gandhi, R. B.; Raghavan, K. Grouping solvents by statistical analysis of solvent property parameters: implication to polymorph screening. *Int. J. Pharm.* 2004, *283* (1–2), 117-125.

47. Vangala, V. R.; Chow, P. S.; Tan, R. B. H. Co-Crystals and Co-Crystal Hydrates of the Antibiotic Nitrofurantoin: Structural Studies and Physicochemical Properties. *Cryst. Growth Des.* 2012, *12* (12), 5925-5938.

48. Braun, D. E.; Karamertzanis, P. G.; Price, S. L. Which, if any, hydrates will crystallise? Predicting hydrate formation of two dihydroxybenzoic acids. *Chem. Commun.* 2011, *47* (19), 5443-5445.

49. Braun, D. E. Experimental and computational approaches to rationalise multicomponent supramolecular assemblies: dapsone monosolvates. *Phys. Chem. Chem. Phys.* 2019, *21* (31), 17288-17305.

50. Iuzzolino, L. Survey of Crystallographic Data and Thermodynamic Stabilities of Pharmaceutical Solvates: A Step toward Predicting the Formation of Drug Solvent Adducts. *Cryst. Growth Des.* 2021, *21* (8), 4362-4371.